STRUCTURAL INTEGRITY ANALYSIS OF NOTCHED FERRITIC STEELS OPERATING WITHIN THEIR DUCTILE-TO-BRITTLE TRANSITION ZONE: AN APPROACH FROM FAILURE ASSESSMENT DIAGRAMS AND THE NOTCH MASTER CURVE

S. Cicero[1,*], T. García[1], V. Madrazo[2]

1) Dpto. Ciencia e Ingeniería del Terreno y de los Materiales, Universidad de Cantabria, Av/ Los Castros 44, 39005, Santander, Cantabria, Spain
2) Fundación Centro Tecnológico de Componentes (CTC), Parque Científico y Tecnológico de Cantabria (PCTCAN), C/ Isabel Torres nº 1, 39011, Santander, Spain
*corresponding author: ciceros@unican.es

Abstract

This paper provides a structural integrity assessment methodology for the analysis of ferritic steels containing notch-type defects and operating within their ductile-to-brittle transition zone. The methodology, based on the use of Failure Assessment Diagrams and the novel concept of the Notch Master Curve, has been applied to 323 experimental results performed on four different steels (S275JR, S355J2, S460M and S690Q), six different notch radii (from 0 mm up to 2.0 mm), two different types of specimens (CT and SENB), and three different temperatures within the corresponding ductile-to-brittle transition zone. The results validate the proposed assessment methodology.

Keywords: ferritic steel, notch effect, Master Curve, Failure Assessment Diagram, Notch Master Curve, Theory of Critical Distances

1. INTRODUTION: NOTCH EFFECT, FAILURE ASSESSMENT DIAGRAMS AND THE NOTCH MASTER CURVE

1.1. Notch effect and the Theory of Critical Distances

As is widely reported in the literature (e.g. [1-9]), notched components develop a greater fracture resistance than that developed in cracked conditions. This may have direct consequences on the load-bearing capacity of the component, and also on the corresponding structural integrity. Consequently, the development of methodologies for the assessment of the notch effect would reduce the conservatism in many practical situations where the not sharp existing defects (e.g. corrosion defects, fabrication defects, structural details, etc.) are treated as if they were cracks.

There are different failure criteria in notch theory (e.g. [2, 3]). Among them, this research is exclusively focussed on two local criteria included within the Theory of Critical Distances (TCD): the Point Method (PM) and the Line Method (LM). Both of them use a characteristic material length parameter (the critical distance, L) when performing fracture assessments [8]:

$$L = \frac{1}{\pi}\left(\frac{K_{mat}}{\sigma_0}\right)^2 \quad (1)$$

K_{mat} is the material fracture toughness and σ_0 is a characteristic material strength parameter (the inherent strength) that must be calibrated (except for those materials with linear-elastic behaviour at both the macro and the micro scales, where σ_0 coincide with the ultimate tensile strength, σ_u [8]).

The PM [10] establishes that fracture occurs when the stress reaches the inherent strength (σ_0) at a distance from the defect tip equal to *L/2*:

$$\sigma\left(\frac{L}{2}\right)=\sigma_0 \tag{2}$$

The LM [11] assumes that fracture occurs when the average stress along a distance equal to *2L* (starting from the defect tip), reaches the inherent strength, σ_0:

$$\frac{1}{2L}\int_0^{2L}\sigma(r)dr=\sigma_0 \tag{3}$$

These two methodologies may generate predictions of the apparent fracture toughness (K^N_{mat}) exhibited by components containing U-shaped notches. This requires assuming the stress distribution on the notch tip provided by Creager and Paris [12]:

$$\sigma(r)=\frac{K_I}{\sqrt{\pi}}\frac{2(r+\rho)}{(2r+\rho)^{3/2}} \tag{4}$$

Where K_I is the stress intensity factor (as defined for a crack with the same geometry), *r* is the distance from the notch tip and ρ is the notch radius. Now, considering the PM fracture condition (equation (2)), the definition of the critical distance *L* (equation (1)), and establishing that failure takes place when K_I is equal to K^N_{mat}, equation (5) is obtained [8]:

$$K^N_{mat}=K_{mat}\frac{\left(1+\frac{\rho}{L}\right)^{3/2}}{\left(1+\frac{2\rho}{L}\right)} \tag{5}$$

Likewise, the application of the LM provides equation (6):

$$K^N_{mat}=K_{mat}\sqrt{1+\frac{\rho}{4L}} \tag{6}$$

1.2. Failure Assessment Diagrams

Failure Assessment Diagrams (FADs) are one of the main engineering tools for the assessment of fracture-plastic collapse processes in cracked components (e.g. [13-17]). These diagrams

present a simultaneous assessment of both fracture and plastic collapse processes representing the component through coordinates K_r and L_r, whose expressions are:

$$K_r = \frac{K_I}{K_{mat}} \tag{7}$$

$$L_r = \frac{P}{P_L} \tag{8}$$

P is the applied load, P_L is the limit load, K_I is the stress intensity factor, and K_{mat} is the material fracture resistance measured by the stress intensity factor. The BS7910 [14] also defines L_r as the ratio between the reference stress (σ_{ref}) and the yield strength (σ_Y), this definition being totally analogous to that represented by equation (8).

In any case, it may be observed that L_r evaluates the situation against plastic collapse, whereas K_r evaluates the component against fracture. Once the assessment point of the component is defined through the coordinates (K_r,L_r), it is necessary to define the failure conditions. With this purpose, the Failure Assessment Line (FAL) is defined, so that if the assessment point is located between the FAL and the coordinate axes, the component is considered to be under safe conditions, whereas if the assessment point is located above the FAL, the component is considered to be under unsafe conditions. The critical situation (failure) is that in which the assessment point lies exactly on the FAL, whose general expression is:

$$K_r = f(L_r) \tag{9}$$

Figure 1[9] shows an example of this kind of assessment, where the crack-like assessment of the defect leads to unsafe conditions (the assessment point is located above the FAL).

1.3. The Notch Master Curve

The Master Curve (MC) [17-21] is a fracture characterisation tool for cracked ferritic steels operating within their ductile-to-brittle transition zone (DBTZ). It is based on statistical considerations related to the distribution of cleavage promoting particles around the crack tip, and assumes that cleavage fracture of ferritic steels is activated by the presence of such particles Therefore, fracture is basically an initiation dependent process which, consequently, is assumed to be controlled by weakest link statistics and follows a three parameter Weibull distribution. Hence, within the scope of small-scale yielding conditions, the cumulative failure probability (P_f) on which the MC is based follows equation (10):

$$P_f = 1 - e^{-\frac{B}{B_0}\left(\frac{K_{Jc}-K_{\min}}{K_0-K_{\min}}\right)^b} \tag{10}$$

K_{Jc} is the fracture toughness for the selected failure probability (P_f), K_0 is a scale parameter located at the 63.2 % cumulative failure probability level, B is the specimen thickness and B_0 is the reference specimen thickness assumed in this methodology (B_0 = 25 mm, also referred to as 1T). K_{min} and b take the same values for all ferritic steels and have been experimentally fitted,

providing 20 MPam$^{1/2}$ and 4 respectively. Thus, the fracture characterisation within the DBTZ is performed by using K_{Jc}, which is an elastic-plastic equivalent stress intensity factor derived from the *J*-integral at the point of onset of cleavage fracture, J_c.

The dependence of K_0 on temperature under cleavage fracture conditions follows equation (11) [11-13,27]:

$$K_0 = 31 + 77e^{0.019\cdot[T-T_0]} \tag{11}$$

T_0 is the reference temperature, corresponding to the temperature where the median fracture toughness for a 25 mm thick specimen is 100 MPam$^{1/2}$. Therefore, the only parameter required to define the temperature dependence of K_{Jc} is the material reference temperature. Whichever the ferritic steel is, and once the corresponding T_0 is known, it is possible to define the MC for any probability of failure (P_f):

$$K_{Jc,P_f} = 20 + \left(-\ln\left(1-P_f\right)\right)^{0.25}\left[11 + 77e^{0.019(T-T_0)}\right] \tag{12}$$

The experimental and analytical procedure that allows T_0 to be determined is gathered in [21]. Moreover, when the specimen or component thickness is not 25 mm, [21] provides equation (13) relating the fracture toughness value for a 25 mm thick specimen (B_0) with the fracture toughness value corresponding to any other thickness (B_x):

$$K_{Jc(x)} = 20 + \left[K_{Jc(0)} - 20\right]\left(\frac{B_0}{B_x}\right)^{1/4} \tag{13}$$

$K_{Jc(x)}$ being the value of K_{Jc} for a specimen thickness of B_x.. Thus, when predicting the fracture toughness in a specimen whose thickness is B_x, and for a given probability of failure (P_f), equations (12) and (13) can be combined, providing equation (14):

$$K_{Jc(x)} = 20 + \left[\left(-\ln\left(1-P_f\right)\right)^{0.25}\left[11 + 77e^{0.019(T-T_0)}\right]\right]\left(\frac{B_0}{B_x}\right)^{1/4} \tag{14}$$

The curves associated to probabilities of failure of 95%, 50% and 5% are, respectively, those gathered in equations (15), (16) and (17):

$$K_{Jc(x)0.95} = 20 + \left[14.5 + 101.3\cdot e^{0.019(T-T_0)}\right]\left(\frac{B_0}{B_x}\right)^{1/4} \tag{15}$$

$$K_{Jc(x)0.50} = 20 + \left[10 + 70\cdot e^{0.019(T-T_0)}\right]\left(\frac{B_0}{B_x}\right)^{1/4} \tag{16}$$

$$K_{Jc(x)0.05} = 20 + \left[5.2 + 36.6 \cdot e^{0.019(T-T_0)}\right]\left(\frac{B_0}{B_x}\right)^{1/4} \quad (17)$$

For those situations on which ferritic steels contain notches (instead of cracks), the authors have previously proposed [22,23] the Notch Master Curve (NMC). It arises from the combination of the MC and the TCD and its main assumptions may be consulted in [22,23]. For a given thickness (B_x) these would be equations (18) to (20):

$$K^N_{Jc(x)0.95} = \left[20 + \left[14.5 + 101.3 \cdot e^{0.019(T-T_0)}\right]\left(\frac{B_0}{B_x}\right)^{1/4}\right] \cdot \sqrt{1 + \frac{\rho}{4L}} \quad (18)$$

$$K^N_{Jc(x)0.50} = \left[20 + \left[10 + 70 \cdot e^{0.019(T-T_0)}\right]\left(\frac{B_0}{B_x}\right)^{1/4}\right] \cdot \sqrt{1 + \frac{\rho}{4L}} \quad (19)$$

$$K^N_{Jc(x)0.05} = \left[20 + \left[5.2 + 36.6 \cdot e^{0.019(T-T_0)}\right]\left(\frac{B_0}{B_x}\right)^{1/4}\right] \cdot \sqrt{1 + \frac{\rho}{4L}} \quad (20)$$

It is important to notice that the subscripts 0.95, 0.50 and 0.05 indicate that the corresponding apparent fracture toughness predictions come from the MC estimations associated to probabilities of failure of, respectively, 95%, 50% and 5%, but they do not necessarily imply such exact probabilities of failure, given that the notch effect is simply fitted through the least squares methodology (as shown below). In any case, the 0.95 and 0.05 NMC predictions may be considered as upper and lower bound estimates (respectively) of the apparent fracture toughness.

As it may be seen from equations (18) to (20), the application of the NMC requires determining T_0, which is obtained by testing cracked specimens following [21], and the value of L along the DBTZ.

2. COMBINING FADs AND THE NOTCH MASTER CURVE FOR THE STRUCTURAL INTEGRITY ASSESSMENT OF NOTCHED COMPONENTS

The notch assessment methodology proposed here combines the FAD methodology [7] with the NMC predictions, through the introduction of the latest in the K_r parameter. Thus, the definition of the K_r parameter in notch analysis would be:

$$K_r = \frac{K_I}{K^N_{Jc}} \quad (21)$$

If the LM is applied, together with the $K^N_{Jc(x)0.05}$ predictions, the corresponding equations would be:

$$K_r = \frac{K_I}{K^N_{Jc(x)0.05}} = \frac{K_I}{\left[20 + \left[5.2 + 36.6 \cdot e^{0.019(T-T_0)}\right] \cdot \left(\frac{B_0}{B_x}\right)^{1/4}\right] \cdot \sqrt{1 + \frac{\rho}{4L}}} \quad (22)$$

Analogous expressions would be obtained when using the PM corrections. In any case, regardless of the expression being used for K^N_{Jc}, this methodology proposes the conversion of a notched material with K_{Jc} as the fracture resistance into an equivalent situation with a cracked material having a higher fracture resistance, equal to K^N_{Jc} (i.e., the K_I solutions are the same as those used in cracked geometries).

This approach is analogous to that proposed by the authors in [7,9], with the particularity of using the NMC for the prediction of the apparent fracture toughness all along the DBTZ, instead of applying a particular correction provided by the TCD for every single temperature. Thus, the methodology presented here constitutes a more general solution for the assessment of notched ferritic steels, with general application within the whole DBTZ, whereas the approach gathered in [7,9] is only applicable at the specific temperatures where L has been calibrated and defined

As also explained in [7,9], in order to complete the FAD analysis it is necessary to define the L_r parameter, which depends on the limit load (equation (8)). Plastic collapse occurs through the yielding of the remnant section, so that, in a perfectly plastic material, it can be defined by the material yield stress and the defect dimensions, with no influence of the radius existing on the defect tip. In [24] the low influence of the notch radius on the limit load is demonstrated. Hence, L_r is determined in the same way it is calculated for cracked components.

Finally, Horn and Sherry [25, 26] have demonstrated a weak dependence of failure assessment lines (FALs) on the notch radius. These authors state that this independence does not contradict experimental observations of increasing resistance to fracture with increasing notch radius, given that the benefit associated with increasing notch radius is quantified by the increase in the notch (apparent) fracture toughness. Consequently, FAL solutions are the same as those used for cracked components.

With all this, the only change proposed here when performing assessments on notched components (if compared to cracked components) affects the definition of K_r. If this methodology is compared to the assessment of notches as if they were cracks (a conservative practice, as mentioned above), equation (22) would produce a reduction of the K_r parameter and, then, a vertical displacement of the assessment point, as shown in Figure 1.

There are other proposals for the notch correction in FAD analysis, the reader being referred to the literature to obtain a detailed description of them (e.g. [25-28]).

3. MATERIALS AND METHODS

The methodology proposed here for the assessment of notches through Failure Assessment Diagrams and the NMC predictions for the apparent fracture toughness has been applied to four ferritic steels: S275JR, S355J2, S460M and S690Q. This constitutes a wider coverage than that gathered in [9], which was restricted to ferritic steels S275JR and S355J2. As stated in [21],

ferritic steels are typically carbon, low-alloy, and higher alloy grades, whose typical microstructures are bainite, tempered bainite, tempered martensite, and ferrite and pearlite. A brief description of the four materials and the corresponding specimens is gathered here:

- Steel S275JR: 84 CT 25 mm thick specimens are considered here (Figure 2). A complete description of the experimental procedure may be found in [22]. Here, it is sufficient to say that the 84 specimens cover 6 different notch radii, and three different temperatures belonging to the DBTZ (-10ºC, -30ºC and -50ºC). The material presents a ferritic-pearlitic microstructure [29].

- Steel 355J2: again, 84 CT 25 mm thick specimens are considered here (Figure 2), covering 6 different notch radii, and three different temperatures belonging to the DBTZ (-100ºC, -120ºC and -150ºC). The description of the experimental procedure may be found in [22]. The material presents a ferritic-pearlitic microstructure [29].

- Steel S460M: 84 SENB 15 mm thick specimens (Figure 2), covering the same 6 notch radii, and three different temperatures belonging to the DBTZ (-100ºC, -120ºC and -140ºC). The experimental procedure is described in [23]. The material presents a ferritic-pearlitic microstructure [23].

- Steel S690Q: 84 SENB 15 mm thick specimens (Figure 2), covering the same 6 notch radii and testing temperatures of steel S460M. The experimental procedure is described in [23]. The material microstructure is composed by bainite and tempered martensite [23].

The nominal notch depth is 25 mm for all the specimens, although crack depths may be slightly different. Tables 1 and 2 present a description of the specimen conditions and the corresponding load- bearing capacities, while Table 3 presents the value of the main mechanical properties, the reference temperature (T_0) and the average value of the critical distance (L) along the DBTZ [22]. The latter has been obtained, firstly, through the best fit (least squares) of the apparent fracture toughness experimental results (e.g. see Figure 3) at each testing temperature and, secondly, as the average of the three values of L obtained for each material. It may be observed from tables 1 and 2 that 13 of the tests were not valid, so there are 323 valid tests.

The reference temperatures, T_0, of the four steels were obtained applying the ASTM 1921-13 [21] to the corresponding cracked specimens and following the multi-temperature option. The apparent fracture toughness results obtained in notched specimens, used in the calibration process of L (e.g. Figure 3), were obtained following the procedure specified in [21,30] for the determination of K_{Jc} in cracked specimens:

$$K_{Jc}^{N} = \sqrt{J_c^{N} \frac{E}{1-\nu^2}} \tag{23}$$

where J^N_c is the apparent J-integral at onset of cleavage fracture, E is the Young´s modulus and ν is the Poisson´s ratio [21,30]:

$$J_c^N = J_e^N + J_p^N = \frac{\left(1-\nu^2\right)\left(K_e^N\right)^2}{E} + \frac{\eta A_p}{Bb_0} \tag{24}$$

where J^N_e and J^N_p are, respectively, the elastic and plastic components of J^N_c, η is a dimensionless constant, A_p is the plastic area under the load-displacement curve, b_0 is the initial remaining ligament and K^N_e is the apparent elastic stress intensity factor at instability [21,30]. Therefore K^N_{Jc} values are obtained at the onset of cleavage.

With all this, the assessment requires the following steps:

- Definition of the Failure Assessment Line: the solution provided by Option 1 of BS7910 [14] will be used here. It requires knowing the yield strength (σ_Y), the ultimate tensile strength (σ_u) and the elastic modulus (E), all of them gathered in Table 3. Steels S460M and S690Q do not exhibit yield plateau, so that the corresponding equations are:

$$K_r = f(L_r) = \left[1+\frac{1}{2}(L_r)^2\right]^{-1/2}\left[0.3+0.7\cdot\exp\left(-\mu L_r^6\right)\right] \qquad L_r \leq 1 \tag{25}$$

$$K_r = f(L_r) = f(1)\cdot L_r^{\frac{N-1}{2N}} \qquad 1 < L_r < L_{r,max} \tag{26}$$

$$K_r = f(L_r) = 0 \qquad L_r \geq L_{r,max} \tag{27}$$

$$\mu = \min\left[0.001\frac{E}{\sigma_Y};0.6\right] \tag{28}$$

$$N = 0.3\left(1-\frac{\sigma_Y}{\sigma_u}\right) \tag{29}$$

$$L_{r,\max} = \frac{1}{2}\frac{\sigma_Y+\sigma_u}{\sigma_Y} \tag{30}$$

On their part, steels S275JR and S355J2 exhibit yield plateau. Thus, following [14] equations (25) to (27) should be replaced by equations (31) to (34):

$$K_r = f(L_r) = \left(1+\frac{1}{2}(L_r)^2\right)^{-1/2} \qquad L_r < 1 \tag{31}$$

$$K_r = f(L_r) = \left(\lambda+\frac{1}{2\lambda}\right)^{-1/2} \qquad L_r = 1 \tag{32}$$

$$K_r = f(L_r) = f(1)\cdot L_r^{\frac{N-1}{2N}} \qquad 1 < L_r < L_{rmax} \tag{33}$$

$$K_r = f(L_r) = 0 \qquad L_r \geq L_{r,max} \tag{34}$$

With λ and $\Delta\varepsilon$ following equations (35) and (36), respectively:

$$\lambda = \left(1+\frac{E\cdot\Delta\varepsilon}{\sigma_Y}\right) \tag{35}$$

$$\Delta\varepsilon = 0.0375\left(1 - 0.001\cdot\sigma_Y\right) \quad (36)$$

In equations (25) to (36), σ_Y refers to the proof strength ($R_{p0.2}$, for continuous yielding) or to the lower yield stress (R_{eL}, for discontinuous yielding).

- Definition of K_r: as explained above, this parameter refers to the ratio between the stress intensity factor and the material fracture resistance. The stress intensity factor solutions for CT and SENB specimens in cracked conditions will be taken from [17], with the applied load being the load bearing capacity gathered in tables 1 and 2, whereas the fracture resistance values will be those provided by the Notch Master Curve. Thus, K_r follows equation (22), with the T_0 and L values gathered in Table 3. Given that K^N_{Jc} values are obtained at the onset of cleavage fracture, the structural integrity assessment performed here correspond to such physical situation.

- Definition of L_r: it is the ratio between the applied load on each specimen (load bearing capacity, as gathered in tables 1 and 2) and the limit load solutions provided in [17] for cracked geometries.

  Here it should be noted that when the notch radius increases, the specimen conditions may vary from plain strain conditions in cracked conditions up to plain stress conditions for those specimens with higher radii (e.g, [8,9]).

  When the notch fracture toughness (K^N_{mat}) associated to a particular material, notch radius and temperature is lower than the value provided by equation (37) [8], then it is assumed that plain strains conditions are dominant, and the corresponding P_L solutions are given by equations (38) and (39) for CT and SENB specimens, respectively [17]:

$$K^N_{mat}\left[\text{ plane - strain limit }\right] = \sigma_Y\left(B/2.5\right)^{0.5} \quad (37)$$

$$P_L = 1.455\eta B b \sigma_f \quad (38)$$

$$P_L = \frac{1.455 B b^2 \sigma_f}{S} \quad (39)$$

  where B is the thickness of the specimen, b is the remaining ligament, S is the span, σ_f is the flow stress (average between the yield strength and the ultimate tensile strength) and η follows equation (40):

$$\eta = \sqrt{\left(\frac{2a}{b}\right)^2 + \frac{4a}{b} + 2} - \left(\frac{2a}{b} + 1\right) \quad (40)$$

  where a is the defect size.

  On the other hand, when K^N_{mat} values are higher than the limit established by equation (41) [8], it is considered that plane stress conditions are dominant, the P_L solutions

being those provided by equations (42) and (43), respectively, for CT and SENB specimens:

$$K_c^N\left[\text{ plane - stress onset }\right]=\sigma_Y\left(\pi B\right)^{0.5} \tag{41}$$

$$P_L=1.072\eta Bb\sigma_f \tag{42}$$

$$P_L=\frac{1.072Bb^2\sigma_f}{S} \tag{43}$$

For those situations located between the limits established by equations (37) and (41), the P_L solution has been obtained by interpolation between equations (38) and (42), in case of CT specimens, or between equations (39) and (43), in case of SENB specimens.

4. RESULTS

This section shows the FAD analysis of the 323 CT specimens included in the experimental program, with and without the notch correction proposed in this paper (equation (22)).

Figures 4, 5, 6 and 7 present the results for steels S275JR, S355J2, S460M and S690Q, respectively. Figure 4a presents a circle with some assessment points located on the left side. These points correspond to the cracked specimens, for which the two assessment conditions (crack-like and notch) provide the same location of the assessment points. For the sake of simplicity, this circle is not represented in the rest of the figures. Also, it should be noticed that the higher the notch radius the larger the distance from the crack-like assessment points to the FAL.

The results for steel S275JR reveal that the methodology proposed here significantly reduces the conservatism of the analysis, given that the assessment points at failure are located much closer to the failure condition (represented by the FAL) once the notch correction is applied. The improvement of the results is more significant at -50 ºC. Also, it is important to notice that, although the conservatism (measured as the distance from the assessment points to the FAL) is noticeably reduced, there are no unsafe results (i.e., none of the specimens at failure is represented by a point located within the safe area of the FAD).

Concerning steel S355J2, the results are quite similar to those obtained in steel S275JR: the application of the notch correction improves the accuracy of the assessments (i.e., the assessment points are located closer to the FAL). Again, the improvement is more significant at the lower temperature (-150ºC), although on this occasion there are two unsafe results, given that two of the specimens are represented at failure by points located within the safe area. Here, it should be noted that one of these results corresponds to a cracked specimen, so this inconvenience has nothing to do with the notch correction proposed here.

The results obtained in steel S460M also show the accuracy of the proposed methodology, with significant improvements in the results. These improvements take place for the three temperatures being analysed, although at -140 ºC there are a number of points which are basically over the FAL (all the conservatism is eliminated, and the failure predictions are exact).

One of the assessment points is located in the safe area, providing an unsafe result, although the point is very close to the FAL.

Finally, the results of steel S690Q also present noticeable improvements for the three temperatures being analysed. This steel presents the most accurate results (i.e., those closest to the FAL), although this is accompanied by the highest number of unsafe results (3 tests).

With all this, it can be ensured that the methodology proposed here for the assessment of ferritic steels operating in notched conditions within their corresponding DBTZ, provides significant improvements if compared to crack-like assessments. Once the methodology is applied, the assessment points are generally located close to the FAL and seem to follow the shape of the corresponding FADs, demonstrating that the methodology captures adequately the physics of the problem being analysed, and just 6 results (out of 323) are unsafe.

5. CONCLUSIONS

This paper presents a methodology for the assessment of ferritic steels containing notch-type defects and operating within their ductile-to-brittle transition zone. The methodology is based on the Failure Assessment Diagram approach, and maintains the same Failure Assessment Line, stress intensity factor and limit load solutions as those used in crack assessments. The notch correction and the temperature effect are simultaneously considered when defining the material fracture resistance by using the Notch Master Curve, which combines the Master Curve and the notch corrections provided by the Theory of Critical Distances.

The methodology has been applied to 323 experimental results, combining four different steels (S275JR, S355J2, S460M and S690Q), six different notch radii (0 mm, 0.15 mm, 0.25 mm, 0.50 mm, 1.0 mm and 2.0 mm), two types of specimens (CT and SENB) and three different temperatures within the corresponding ductile-to-brittle transition zone.

It has been demonstrated that the methodology proposed here improves significantly the results obtained when the notch nature is not considered (crack-like assessments). The accuracy of the predictions increases and the methodology captures the physics of the problem being analysed, given that the assessment points approach the Failure Assessment Line and seem to follow its shape. Just 6 of the 323 results were unsafe.

ACKNOWLEDGMENTS

The authors of this work would like to express their gratitude to the Spanish Ministry of Science and Innovation for the financial support of the project MAT2010-15721: “Análisis de integridad estructural en defectos tipo entalla” (Structural integrity assessments of notch-type defects), on the results of which this paper is based.

REFERENCES

[1] Niu LS, Chehimi C, Pluvinage G. Stress field near a large blunted V notch and application of the concept of notch stress intensity factor to the fracture of very brittle materials. Eng Fract Mech 1994;49:325-35.

[2] Pluvinage G. Fatigue and fracture emanating from notch; the use of the notch stress intensity factor. Nucl Eng Des 1998;185:173-84.
[3] Bao Y, Jin Z. Size effects and a mean-strength criterion for ceramics. Fatig Fract Eng Mater Struct 1993;16:829-35.
[4] Fenghui W. Prediction of intrinsic fracture toughness for brittle materials from the apparent toughness of notched-crack specimen. J Mater Sci 2000;35:2543-46.
[5] Seweryn A, Łukaszewicz A. Verification of brittle fracture criteria for elements with V-shaped notches. Eng Fract Mech 2002:69:1487-510.
[6] Cicero S, Gutiérrez-Solana F, Álvarez JA. Structural integrity assessment of components subjected to low constraint conditions. Eng Fract Mech 2008;75:3038-59.
[7] Cicero S, Madrazo V, Carrascal IA, Cicero R. Assessment of notched structural components using Failure Assessment Diagrams and the Theory of Critical Distances. Eng Fract Mech 2011;78:2809-25.
[8] Taylor D. The theory of critical distances: a new perspective in fracture mechanics. London: Elsevier; 2007.
[9] Madrazo V, Cicero S, García T. Assessment of notched structural steel components using failure assessment diagrams and the theory of critical distances. Eng Fail Anal 2014;36:104-120.
[10] Peterson RE. Notch sensitivity. In: Sines G, Waisman JL, editors. Metal fatigue, New York: McGraw Hill; 1959. p. 293–306.
[11] Neuber H. Theory of notch stresses: principles for exact calculation of strength with reference to structural form and material. Berlin: Springer Verlag; 1958.
[12] Creager M, Paris C. Elastic field equations for blunt cracks with reference to stress corrosion cracking. Int J Fract 1967;3:247–52.
[13] FITNET Fitness-for-Service (FFS) Proceure - Volume 1. Kocak M, Webster S, Janosch JJ, Ainsworth RA, Koers R, editors., ISBN 978-3-940923-00-4. Printed by GKSS, Germany; 2008.
[14] BS 7910:2013. Guide to methods for assessing the acceptability of flaws in metallic structures. London: British Standard Institution; 2013.
[15] R6, Assessment of the integrity of structures containing defects. British Energy Generation Limited, Rev. 4; 2007.
[16] API 579-1/ASME FFS-1, Fitness-for Service. American Society of Mechanical Engineers; 2007.
[17] Anderson TL. Fracture mechanics: Fundamentals and applications. Florida: CRC Press; 2005.
[18] Wallin K. The scatter in K_{IC} results. Eng Fract Mech 1984;19:1085–93.
[19] Wallin K, Saario T, Törrönen K. Statistical model for carbide induced brittle fracture in steel. Metal Sci 1984;18:13–6.
[20] Wallin K. The size effect in K_{IC} results. Eng Fract Mech 1985;22:149–63.
[21] ASTM 1921-13a. Test method for the determination of reference temperature T_0 for ferritic steels in the transition range. Philadelphia: American Society for Testing and Materials, ASTM; 2013.
[22] Cicero S, Madrazo V, García T. The Notch Master Curve: A proposal of Master Curve for ferritic–pearlitic steels in notched conditions. Eng Fail Anal 2014;42:178-96.
[23] Cicero S, García T, Madrazo V. Application and validation of the Notch Master Curve in medium and high strength structural steels. Eng Fail Anal, Submitted

[24] Miller AG. Review of limit loads of structures containing defects. Int J Pres Ves Pip 1988;32:197-327.
[25] Horn AJ, Sherry AH. An engineering assessment methodology for non-sharp defects in steel structures - Part I: Procedure development. Int J Pres Ves Pip 2012;89:137-50.
[26] Horn AJ, Sherry AH. An engineering assessment methodology for non-sharp defects in steel structures - Part II: Procedure validation and constraint analysis. Int J Pres Ves Pip 2012;89:151-61.
[27] Pluvinage G. Pipe-defect assessment based on the limit analysis, failure-assessment diagram, and subcritical crack growth. Mater Sci 2006;42:127-39.
[28] Matvienko YG. Local fracture criterion to describe failure assessment diagrams for a body with a crack/notch. Int J Fract 2003:124:107-12.
[29] Cicero S, García T, Madrazo V, Carrascal IA, Ruiz E. Analysis of notch effect in load bearing capacity, apparent fracture toughness and fracture micromechanisms of ferritic–pearlitic steels. Eng Fail Anal 2014;44:250-271.
[30] ASTM E1820-11e11. Standard Test Method for Measurement of Fracture Toughness. Philadelphia: American Society for Testing and Materials, ASTM; 2011.

Figures

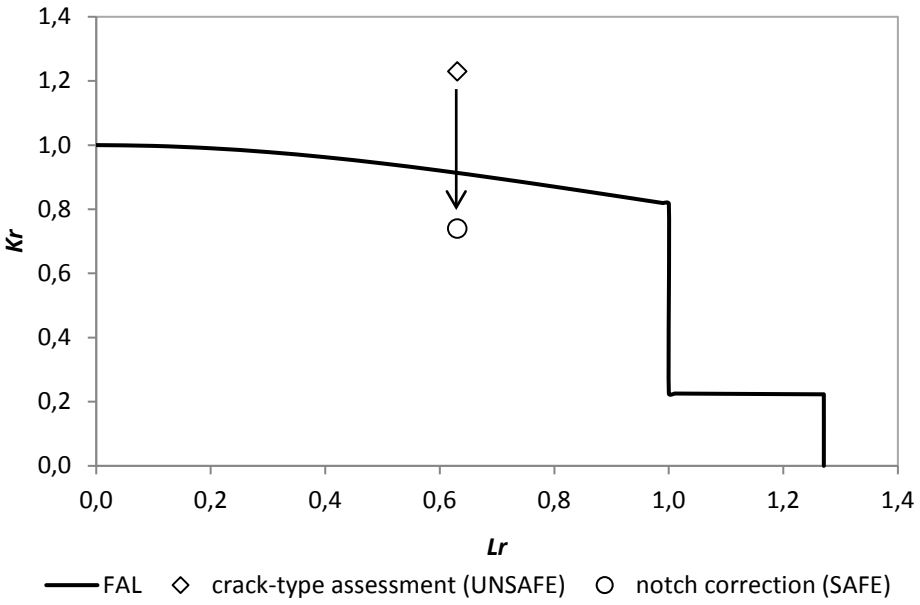

Figure 1. FAD analysis (initiation). The crack-type FAD assessment leads to an unsafe situation; after the application of the notch correction the situation is safe [9].

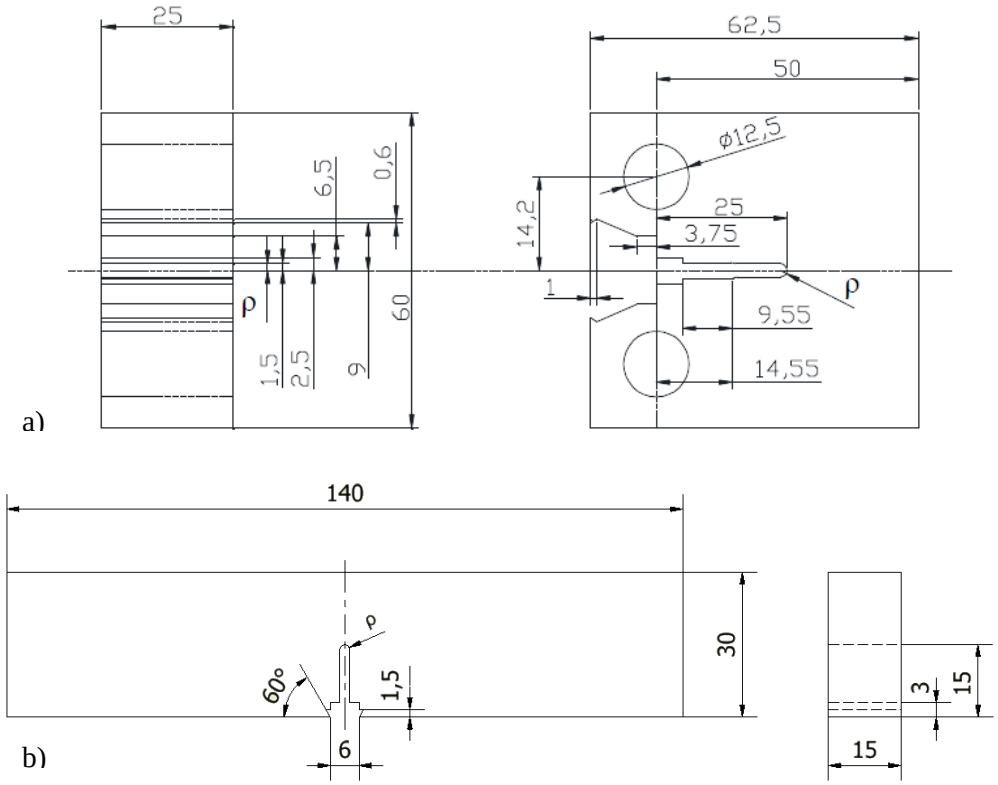

Figure 2. Schematic showing the geometry of the specimens (dimensions in mm). a) CT specimens in steels S275JR and S355J2 [9]; b) SENB specimens in steels S460M and S690Q. ρ varying from 0 mm up to 2.0 mm.

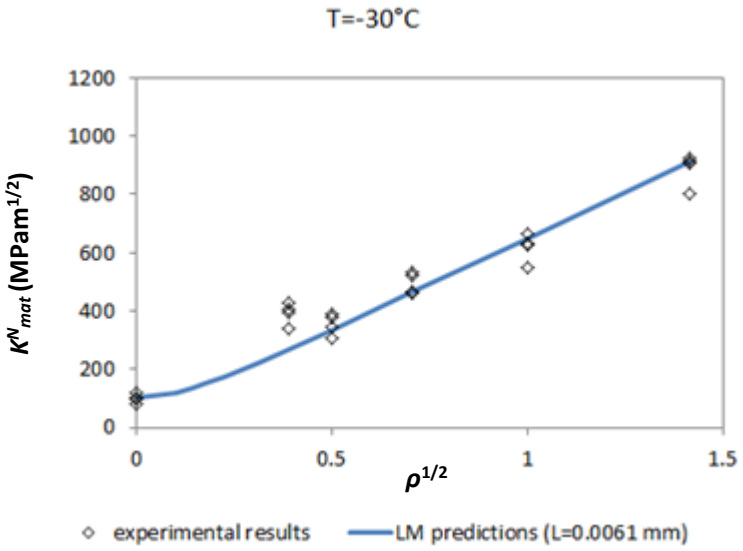

Figure 3. Example of the least squares fitting process used for the calibration of the critical distance, L (Line Method, LM). Steel S275JR at -30ºC. The resulting L is 0.0061 mm, whereas the average L along the DBTZ resulted 0.0064 mm [22].

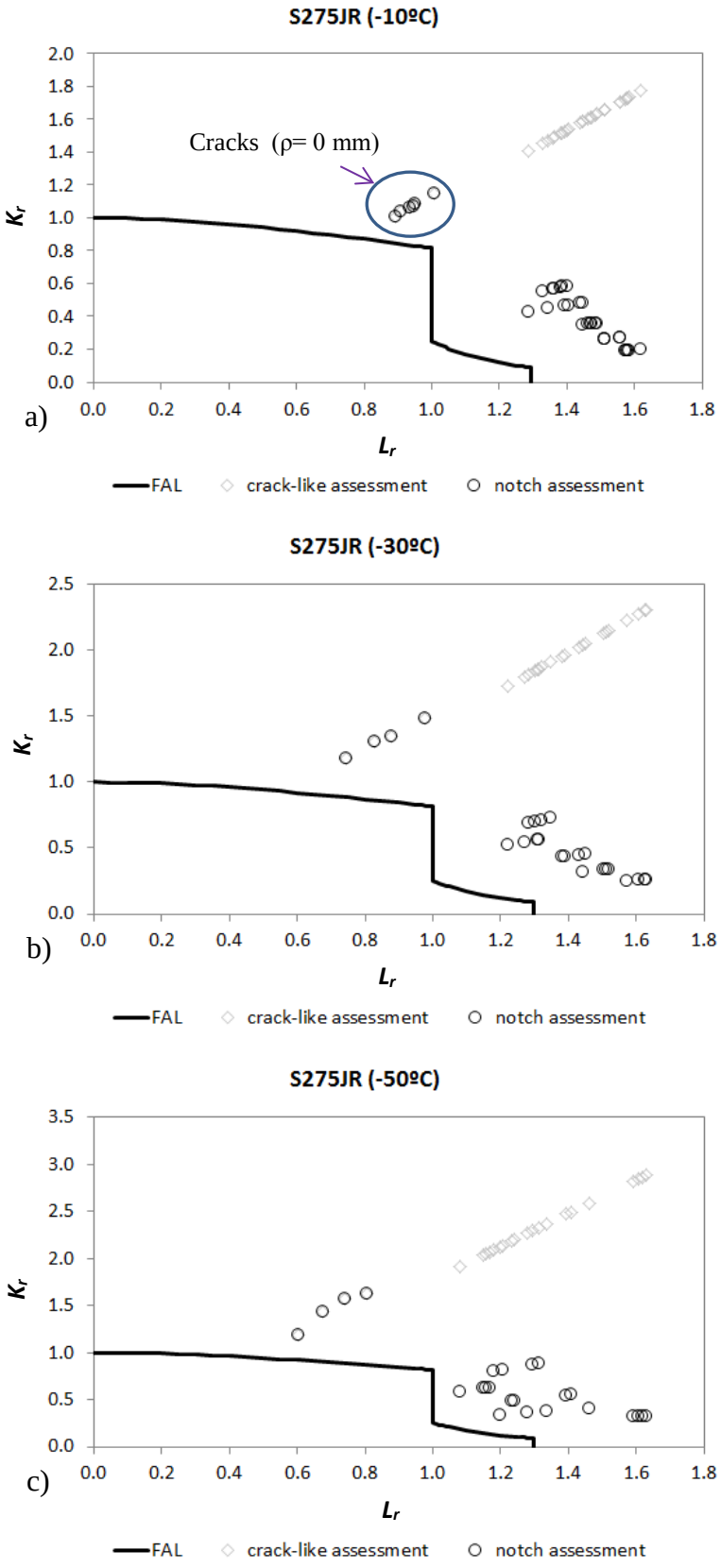

Figure 4. FAD assessment of steel S275JR specimens, showing the results without any notch correction (crack-like assessment), and the results after the notch correction proposed in this paper: a) -10ºC; b) -30ºC; c) -50ºC.

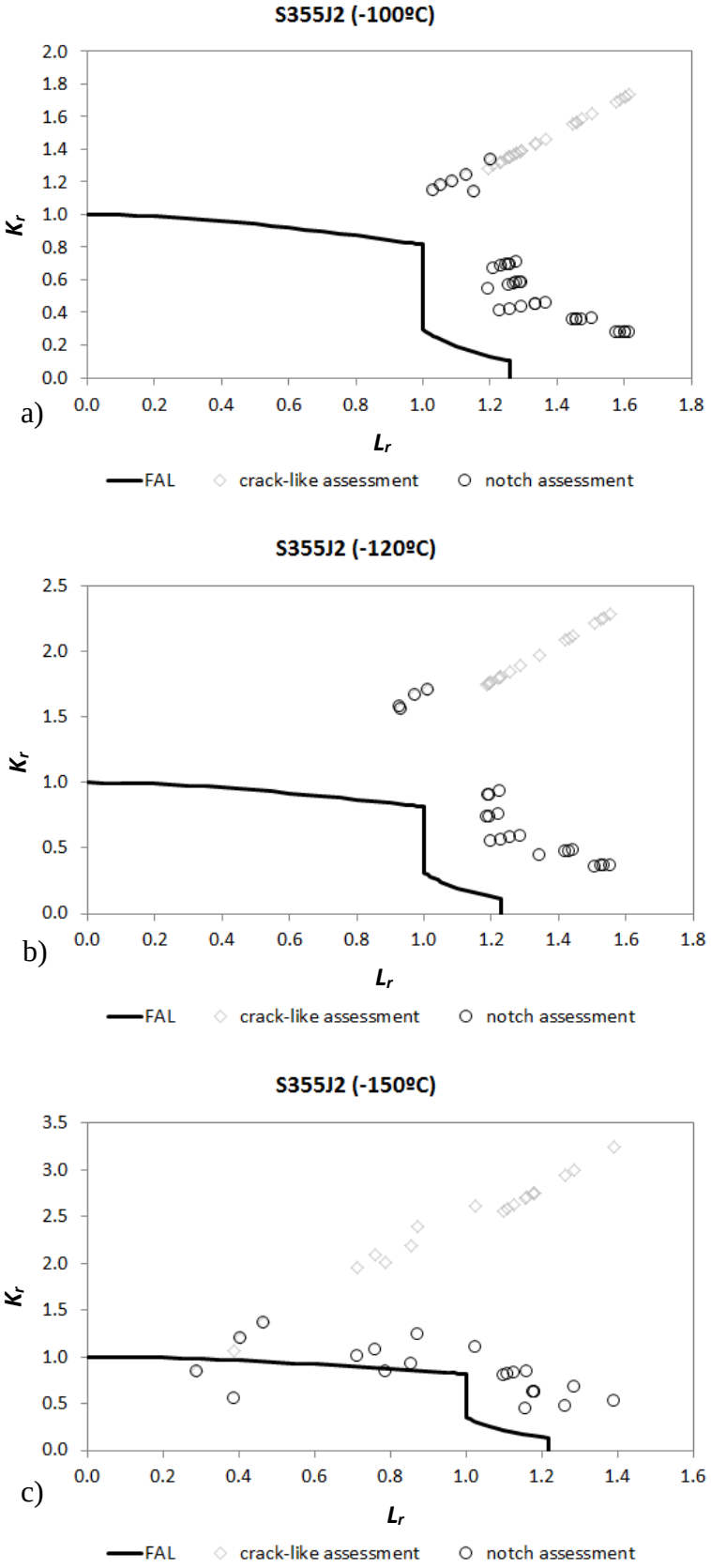

Figure 5. FAD assessment of steel S355J2 specimens, showing the results without any notch correction (crack-like assessment), and the results after the notch correction proposed in this paper: a) -100ºC; b) -120ºC; c) -150ºC.

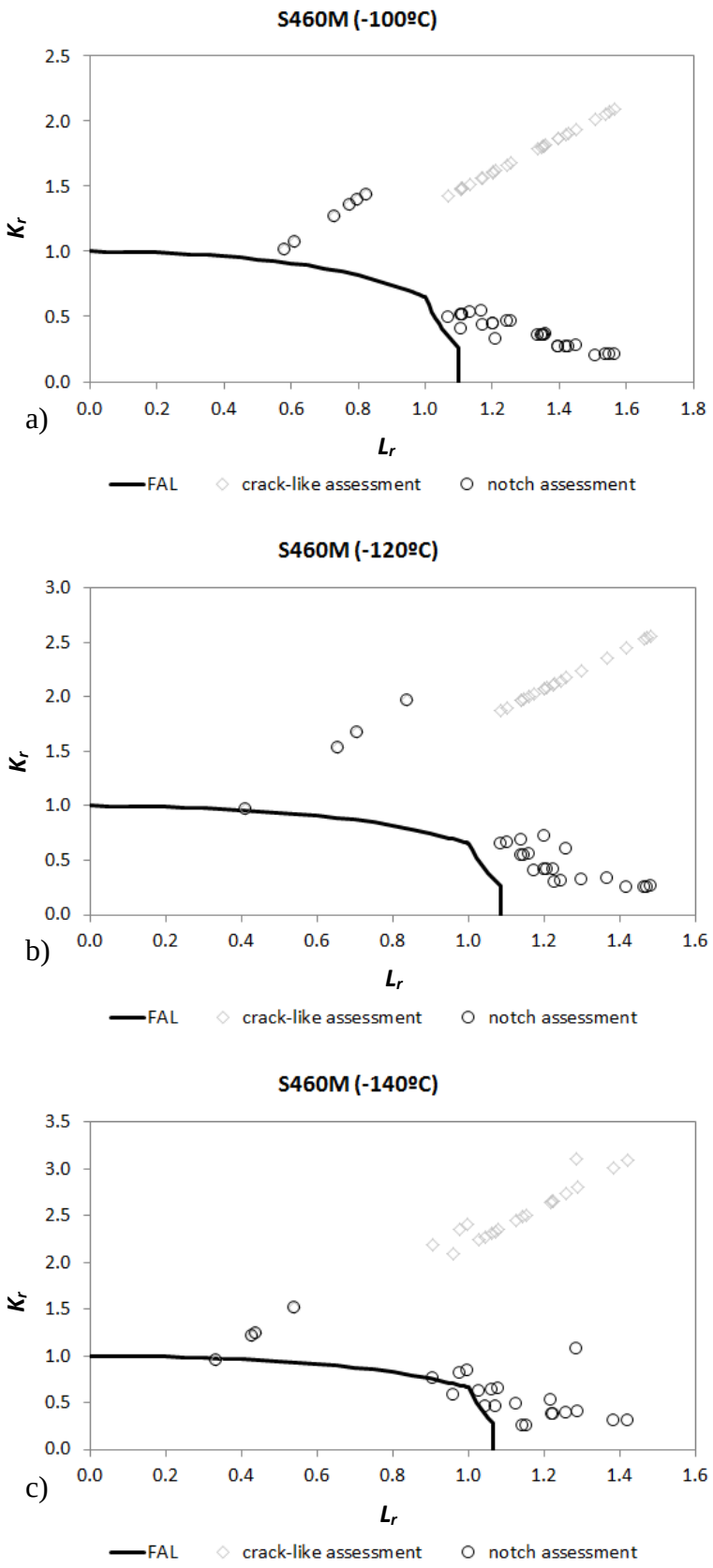

Figure 6. FAD assessment of steel S460M specimens, showing the results without any notch correction (crack-like assessment), and the results after the notch correction proposed in this paper: a) -100ºC; b) -120ºC; c) -140ºC.

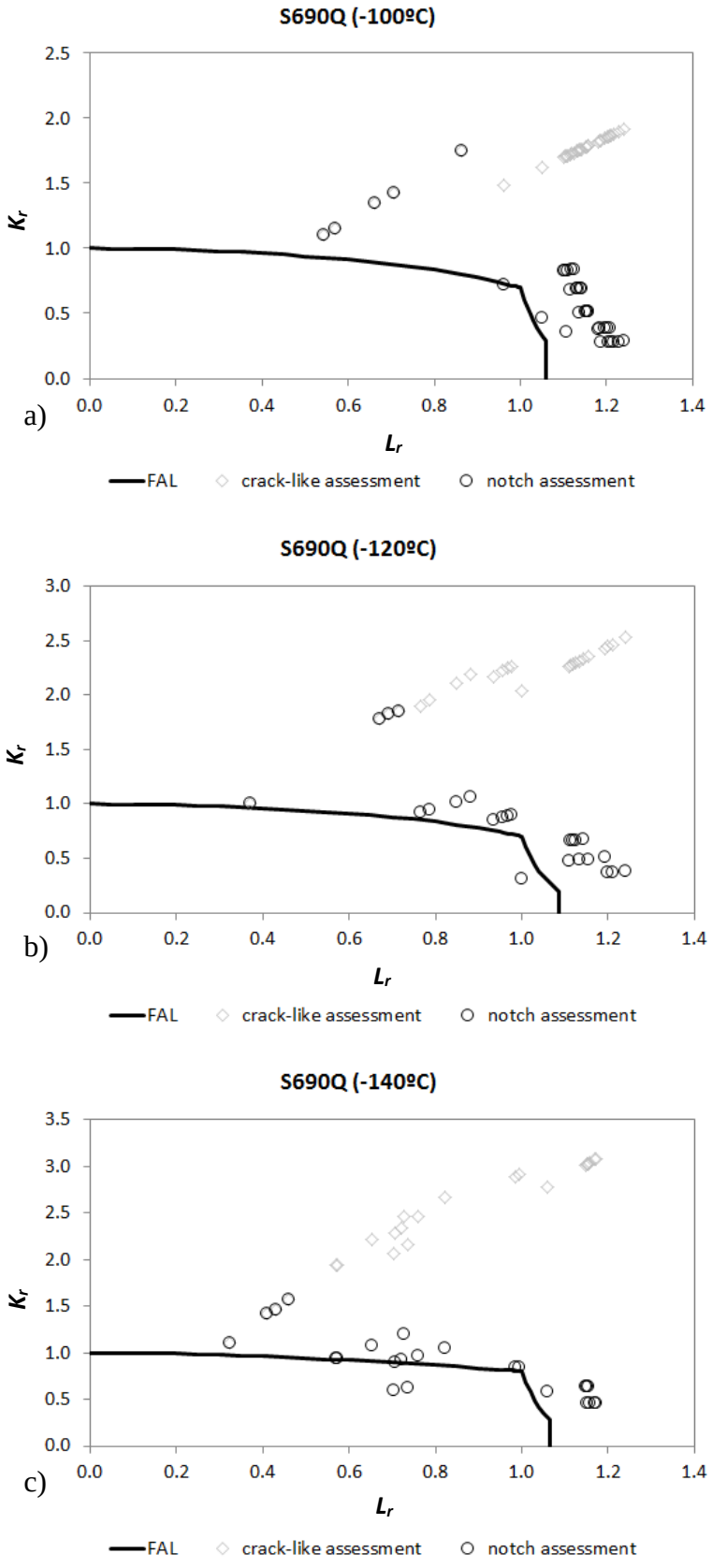

Figure 7. FAD assessment of steel S690Q specimens, showing the results without any notch correction (crack-like assessment), and the results after the notch correction proposed in this paper: a) -100ºC; b) -120ºC; c) -140ºC.

Tables

Table 1. S275JR (2-x) and S355J2 (3-x) specimens, and load bearing capacity (LBC) results

Specimen	Temperature (ºC)	ρ (mm)	LBC (kN)	Specimen	Temperature (ºC)	ρ (mm)	LBC (kN)
2-1	-10	0	43.0	**3-1**	-100	0	54.6
2-2			39.3	**3-2**			54.6
2-3			39.3	**3-3**			53.1
2-4			40.4	**3-4**			61.5
2-5			37.1	**3-5**			61.2
2-6			39.2	**3-6**			55.0
2-7		0.15	63.0	**3-7**		0.15	70.6
2-8			65.8	**3-8**			74.5
2-9			66.4	**3-9**			72.8
2-10			65.6	**3-10**			73.2
2-11			64.4	**3-11**			73.3
2-12			64.6	**3-12**			71.8
2-13		0.25	66.1	**3-13**		0.25	75.2
2-14			63.8	**3-14**			75.3
2-15			66.7	**3-15**			74.1
2-16			68.3	**3-16**			74.6
2-17			68.6	**3-17**			73.2
2-18			61.0	**3-18**			69.7
2-19		0.50	69.4	**3-19**		0.50	71.7
2-20			69.9	**3-20**			77.8
2-21			69.8	**3-21**			79.5
2-22			68.6	**3-22**			73.3
2-23			70.5	**3-23**			75.4
2-24			70.6	**3-24**			77.9
2-25		1.0	-	**3-25**		1.0	87.7
2-26			71.8	**3-26**			84.9
2-27			71.8	**3-27**			85.0
2-28			73.9	**3-28**			84.3
2-29			73.8	**3-29**			85.9
2-30			71.7	**3-30**			85.0
2-31		2.0	74.8	**3-31**		2.0	93.3
2-32			-	**3-32**			93.4
2-33			75.0	**3-33**			94.1
2-34			76.8	**3-34**			92.4
2-35			75.1	**3-35**			91.8
2-36			74.6	**3-36**			-
2-37	-30	0	37.1	**3-37**	-120	0	60.5
2-38			33.6	**3-38**			60.5
2-39			38.5	**3-39**			56.2
2-40			36.0	**3-40**			54.1

2-41		0.15	63.1	**3-41**		0.15	73.3
2-42			65.4	**3-42**			-
2-43			64.1	**3-43**			73.2
2-44			62.1	**3-44**			75.3
2-45		0.25	63.6	**3-45**		0.25	-
2-46			63.4	**3-46**			75.1
2-47			61.6	**3-47**			73.4
2-48			59.2	**3-48**			72.9
2-49		0.50	66.9	**3-49**		0.50	77.1
2-50			69.3	**3-50**			79.1
2-51			70.3	**3-51**			75.4
2-52			67.3	**3-52**			73.7
2-53		1.0	73.2	**3-53**		1.0	87.3
2-54			72.9	**3-54**			87.8
2-55			70.0	**3-55**			88.5
2-56			73.7	**3-56**			82.5
2-57		2.0	79.1	**3-57**		2.0	95.4
2-58			76.3	**3-58**			92.6
2-59			77.9	**3-59**			94.3
2-60			78.9	**3-60**			93.7
2-61	-50	0	24.0	**3-61**	-150	0	-
2-62			38.2	**3-62**			21.0
2-63			34.6	**3-63**			30.4
2-64			34.9	**3-64**			34.4
2-65		0.15	59.9	**3-65**		0.15	71.7
2-66			58.5	**3-66**			31.9
2-67			65.2	**3-67**			62.5
2-68			64.2	**3-68**			58.5
2-69		0.25	57.0	**3-69**		0.25	65.4
2-70			58.0	**3-70**			78.3
2-71			57.4	**3-71**			60.2
2-72			53.6	**3-72**			-
2-73		0.50	61.5	**3-73**		0.50	81.0
2-74			61.1	**3-74**			77.4
2-75			69.8	**3-75**			78.7
2-76			69.2	**3-76**			76.7
2-77		1.0	59.5	**3-77**		1.0	82.4
2-78			66.3	**3-78**			82.1
2-79			63.5	**3-79**			89.8
2-80			72.5	**3-80**			82.4
2-81		2.0	80.8	**3-81**		2.0	97.0
2-82			80.3	**3-82**			-
2-83			79.8	**3-83**			88.1
2-84			78.9	**3-84**			80.8

Table 2. S460M (4-x) and S690Q (6-x) specimens, and load bearing capacity (LBC) results

Specimen	Temperature (ºC)	ρ (mm)	LBC (kN)	Specimen	Temperature (ºC)	ρ (mm)	LBC (kN)
4-1	-100	0	22.01	**6-1**	-100	0	24.21
4-2			16.62	**6-2**			30.61
4-3			22.22	**6-3**			19.57
4-4			16.20	**6-4**			24.39
4-5			19.45	**6-5**			20.41
4-6			21.16	**6-6**			-
4-7		0.15	23.39	**6-7**		0.15	27.90
4-8			22.18	**6-8**			32.56
4-9			22.77	**6-9**			32.45
4-10			21.44	**6-10**			32.15
4-11			22.29	**6-11**			31.92
4-12			22.25	**6-12**			32.02
4-13		0.25	24.96	**6-13**		0.25	33.11
4-14			25.18	**6-14**			32.89
4-15			24.12	**6-15**			32.80
4-16			24.09	**6-16**			33.00
4-17			22.20	**6-17**			32.31
4-18			23.51	**6-18**			-
4-19		0.50	24.30	**6-19**		0.50	32.94
4-20			26.79	**6-20**			30.42
4-21			27.02	**6-21**			33.36
4-22			27.16	**6-22**			33.42
4-23			27.10	**6-23**			33.57
4-24			27.24	**6-24**			33.57
4-25		1.0	29.07	**6-25**		1.0	34.67
4-26			28.02	**6-26**			32.06
4-27			28.03	**6-27**			34.96
4-28			28.51	**6-28**			34.85
4-29			-	**6-29**			34.20
4-30			28.64	**6-30**			34.28
4-31		2.0	-	**6-31**		2.0	35.23
4-32			30.28	**6-32**			34.39
4-33			31.11	**6-33**			35.58
4-34			30.85	**6-34**			34.90
4-35			31.40	**6-35**			35.12
4-36			-	**6-36**			35.97
4-37	-120	0	24.53	**6-37**	-120	0	13.91
4-38			21.34	**6-38**			22.98
4-39			19.02	**6-39**			21.52
4-40			12.40	**6-40**			22.49
4-41		0.15	23.33	**6-41**		0.15	29.00

4-42			24.14	**6-42**			32.54
4-43			22.99	**6-43**			28.23
4-44			25.43	**6-44**			31.24
4-45			24.12	**6-45**			33.37
4-46		0.25	26.67	**6-46**		0.25	33.65
4-47			24.29	**6-47**			33.01
4-48			24.55	**6-48**			32.23
4-49			25.43	**6-49**			34.65
4-50		0.50	24.88	**6-50**		0.50	34.11
4-51			25.94	**6-51**			33.88
4-52			25.57	**6-52**			33.71
4-53			28.94	**6-53**			36.11
4-54		1.0	27.51	**6-54**		1.0	33.63
4-55			26.34	**6-55**			34.37
4-56			26.01	**6-56**			34.95
4-57			31.05	**6-57**			30.32
4-58		2.0	31.40	**6-58**		2.0	37.60
4-59			31.15	**6-59**			36.35
4-60			30.01	**6-60**			36.63
4-61			10.87	**6-61**			11.15
4-62		0	8.80	**6-62**		0	15.09
4-63			11.37	**6-63**			15.45
4-64			13.45	**6-64**			16.21
4-65			32.19	**6-65**			26.87
4-66		0.15	24.98	**6-66**		0.15	23.65
4-67			24.45	**6-67**			29.97
4-68			22.71	**6-68**			23.55
4-69			21.66	**6-69**			27.74
4-70		0.25	24.36	**6-70**		0.25	29.85
4-71			23.23	**6-71**			32.34
4-72	-140		23.94	**6-72**	-140		28.34
4-73			24.15	**6-73**			35.12
4-74		0.50	23.57	**6-74**		0.50	25.13
4-75			25.38	**6-75**			26.22
4-76			27.47	**6-76**			35.47
4-77			27.60	**6-77**			36.80
4-78		1.0	28.41	**6-78**		1.0	36.64
4-79			27.56	**6-79**			33.82
4-80			29.11	**6-80**			36.76
4-81			25.99	**6-81**			37.34
4-82		2.0	25.80	**6-82**		2.0	37.33
4-83			32.07	**6-83**			36.86
4-84			31.22	**6-84**			36.75

Table 3. Main mechanical properties, elastic moduli, reference temperatures (T_0) and critical distances (L) of steels S275JR, S355J2, S460M and S690Q.

	σ_Y (MPa)			σ_u (MPa)			E (GPa)			T_0 (ºC)	L (mm)
Temp. (ºC)	-10	-30	-50	-10	-30	-50	-10	-30	-50	-26.0	0.0064
S275JR	337	344	349	536	548	564	207.0	208.0	209.0		
Temp. (ºC)	-100	-120	-150	-100	-120	-150	-100	-120	-150	-133.0	0.0136
S355J2	426	459	527	646	671	757	212.0	213.2	215.0		
Temp. (ºC)	-100	-120	-140	-100	-120	-140	-100	-120	-140	-91.8	0.0052
S460M	605	647	702	726	758	795	212.0	213.2	214.4		
Temp. (ºC)	-100	-120	-140	-100	-120	-140	-100	-120	-140	-110.8	0.0115
S690Q	907	949	1004	1015	1060	1111	212.0	213.2	214.4		